



## Machine learning revealing key factors influencing HONO chemistry in Beijing during heating and non-heating periods



Wenqian Zhang<sup>a</sup>, Shengrui Tong<sup>a,\*</sup>, Siqi Hou<sup>c</sup>, Pusheng Zhao<sup>d,e</sup>, Yuepeng Pan<sup>f</sup>, Lili Wang<sup>f</sup>, Mengtian Cheng<sup>f</sup>, Dongsheng Ji<sup>f</sup>, Guiqian Tang<sup>f</sup>, Bo Hu<sup>f</sup>, Xin Li<sup>g</sup>, Maofa Ge<sup>a,b</sup>

<sup>a</sup> State Key Laboratory for Structural Chemistry of Unstable and Stable Species, State Key Laboratory for Structural Chemistry of Unstable and Stable Species, Beijing National Laboratory for Molecular Sciences (BNLMS), CAS Research/Education Center for Excellence in Molecular Sciences, Institute of Chemistry, Chinese Academy of Sciences, Beijing 100190, China

<sup>b</sup> University of Chinese Academy of Sciences, Beijing 100049, China

<sup>c</sup> School of Geography Earth and Environment Sciences, University of Birmingham, Birmingham B15 2TT, UK

<sup>d</sup> Joint Laboratory for Electron Microscopy Analysis of Atmospheric Particles, Beijing 100012, China

<sup>e</sup> Beijing Met High-Tech Co., Ltd., Beijing 102200, China

<sup>f</sup> State Key Laboratory of Atmospheric Boundary Layer Physics and Atmospheric Chemistry, Institute of Atmospheric Physics, Chinese Academy of Sciences, Beijing 100029, China

<sup>g</sup> State Key Joint Laboratory of Environmental Simulation and Pollution Control, College of Environmental Sciences and Engineering, Peking University, Beijing 100871, China

### ARTICLE INFO

#### Keywords:

Nitrous acid  
Machine learning  
Random forest  
Heating period  
Non-heating period  
Variable importance

### ABSTRACT

Nitrous acid (HONO) is of great interest due to its contribution to hydroxyl (OH) radicals by self-photolysis. Nowadays, machine learning (ML) algorithms are good at capturing complicated non-linear relationships between predictors and dependent variables. Here, using the whole year of 2018 of observed HONO and related pollutant data at an urban site in Beijing, an ML-RF (random forest) model is carried out to predict HONO concentrations and explore the main factors influencing HONO formation mechanisms. ML-RF models show satisfactory performance during the heating, non-heating and whole year periods with R values of 0.95, 0.96 and 0.95, respectively. Primary emissions and diffusion have an obvious influence on ambient HONO during the heating period, while chemical formation processes such as NO<sub>2</sub> heterogeneous reaction and photolysis of nitrate are important for HONO during the non-heating period with higher RH and stronger solar intensity. O<sub>3</sub> and NH<sub>3</sub> are the most important variables for HONO in both periods, indicating the close relationship of HONO with atmospheric oxidation and the important role of NH<sub>3</sub> in HONO formation processes. Although there are deviations due to some variability in HONO formation mechanisms between years, ML-RF models based on 2018 data are able to roughly predict HONO for three periods in 2017 and 2021. Overall, machine learning with limited meteorological and pollutant parameters offers great advantages in HONO prediction, and it can also provide some clues to improve the chemical mechanisms of HONO by finding related variables of ambient HONO.

### 1. Introduction

Nitrous acid (HONO) is a significant precursor of hydroxyl (OH) radicals. Photolysis of HONO can contribute more than 80% of OH radicals in the atmosphere (Elshorbagy et al., 2010; Kim et al., 2014), especially in the early morning when OH radical formation from O<sub>3</sub> photolysis is low. OH radicals can oxidize most primary pollutants to form secondary aerosols, causing haze and photochemical pollution

(Kleffmann, 2007; Ma et al., 2019). Therefore, HONO is an important gaseous pollutant and has been the subject of much concern. So far, the formation mechanisms of HONO are not well understood and are influenced by meteorological and anthropogenic factors, such as air temperature (Zhang et al., 2023), relative humidity (Stutz et al., 2004), winter heating (Ding et al., 2023), combustion emissions (Chai et al., 2021; Liao et al., 2021; Zhang et al., 2022) and particle concentration (Zhang et al., 2020), and so on. However, these influencing factors on

\* Corresponding author.

E-mail address: [tongsr@iccas.ac.cn](mailto:tongsr@iccas.ac.cn) (S. Tong).

chemical formation mechanisms and emission inventories of HONO are complicated and elusive, which further affects the assessment of atmospheric oxidation capacity and secondary aerosol formation processes.

Chemical transport models and zero-dimensional chemical models have been widely used to study the atmospheric chemistry of HONO, but their performance is highly dependent on the parameterizations of HONO source (Liu et al., 2014; Xue et al., 2022; Zhang et al., 2021; Zhang et al., 2020), which are subject to large uncertainties. In addition, chemical models have limitations in simulating long-term HONO datasets due to high computational costs and/or lack of real-time related pollutants and meteorological parameters (Cui and Wang, 2021). As machine learning (ML) algorithms are now well suited to capture complicated non-linear relationships between predictors and the dependent variables (Grange et al., 2018; Wen et al., 2022; Ye et al., 2022), they have been widely used in air quality studies, such as predicting air pollution (Li et al., 2021; Liang et al., 2022; Philibert et al., 2013; Shi et al., 2021) and improving the underlying mechanisms controlling air pollution in chemical models (Ye et al., 2022). However, ML algorithms are currently rarely used to study atmospheric HONO. Compared to chemical models, the prediction of HONO concentrations by ML algorithms does not require an accurate parameterization scheme of HONO sources, which is now controversial, but is based on a set of related covariates, such as meteorological parameters and pollutant concentrations. Cui and Wang (2021) used the ML model to estimate daily HONO concentrations over China at 0.25° resolution in 2006–2017 using HONO data from a number of previous studies. Nowadays, air quality monitoring stations are distributed all over China, meteorological parameters (such as air temperature, relative humidity, wind speed and wind direction) and conventional pollutant concentrations (such as NO<sub>2</sub>, SO<sub>2</sub>, CO, O<sub>3</sub> and PM<sub>2.5</sub>) are generally available. However, HONO is difficult to measure, because it is extremely active in the atmosphere. ML algorithms offer the possibility of predicting HONO concentrations using available parameters at a specific location, which could be significant for studying local air pollution. To date, there has been no research on HONO prediction by ML using a full year of meteorological parameters and conventional pollutant concentrations in a megacity.

As a megacity in northern China, Beijing has highly variable meteorological conditions and anthropogenic emissions throughout the year. For example, the air temperature drops significantly from late autumn, and full heating starts from November 15 to March 15 of the following year. The heating period includes late autumn, winter and early spring, which are usually accompanied by low temperatures, high wind speeds and northerly winds. In addition to meteorological conditions, anthropogenic activities also differ from the non-heating period. For example, the preference for motor vehicle travel leads to more vehicle emissions in the cold season, and primary pollutants may increase due to the combustion of coal and biomass for heating around Beijing. Due to significant differences in meteorological conditions and anthropogenic factors, the formation mechanisms of HONO should be different between the heating and non-heating seasons. Few studies have investigated the differences in HONO formation mechanisms between the heating and non-heating seasons in megacities such as Beijing.

In this study, we have measured air temperature (temp), relative humidity (RH), wind speed (WS), wind direction (WD), gaseous HONO and related pollutants (NO<sub>2</sub>, O<sub>3</sub>, SO<sub>2</sub>, CO, NH<sub>3</sub>, PM<sub>2.5</sub> and nitrate in PM<sub>2.5</sub>) at an urban site in Beijing during 2018. An ML-based random forest (RF) algorithm is established to explore the influences of meteorology and related pollutants on HONO sources, and to identify the main factors influencing ambient HONO during the heating and non-heating seasons. In addition, to confirm the predictive performance of ML algorithms and to explore the differences in HONO formation mechanisms between years, the 2018 machine learning-based random forest (ML-RF) model is used to predict HONO concentrations for three periods in 2017 and 2021. This study analyzes the feasibility of machine learning in predicting HONO using commonly observed pollutant concentrations

and meteorological parameters from monitoring sites, and attempts to provide an idea for improving HONO formation mechanisms in chemical models.

## 2. Measurement and method

### 2.1. Measurement instruments and sampling site

In this study, the hourly time-resolved quantification of HONO, NH<sub>3</sub>, SO<sub>2</sub> and nitrate in PM<sub>2.5</sub> is measured using the commercial MARGA (Monitor for AeRosols and Gases in ambient Air, Metrohm Ltd., Switzerland). Ambient air is drawn into the sample box by an air pump at a flow rate of 1 m<sup>3</sup> h<sup>-1</sup>. Gases and aerosols are collected by a wet rotating denuder and a steam jet aerosol collector, respectively. An automated ion chromatography system determines the hourly concentrations of the collected samples. The detection limits for HONO, NH<sub>3</sub>, SO<sub>2</sub> and nitrate in PM<sub>2.5</sub> are 0.02, 0.05, 0.03 and 0.05 µg m<sup>-3</sup>, respectively, and the uncertainties for these pollutants are better than 6%. A more detailed description of MARGA can be found in previous studies (Chen et al., 2017; Rumsey et al., 2014; Stieger et al., 2017; Su et al., 2022). Temperature, RH, WS and WD are measured by a Vaisala weather transmitter station (WXT520).

The HONO, NH<sub>3</sub>, SO<sub>2</sub>, nitrate concentrations and meteorological parameters are measured at the Institute of Chemistry, Chinese Academy of Sciences (ICCAS, 39.99°N, 116.32°E), Beijing, China. The ICCAS site is located approximately 10 m above ground level and is surrounded by residential and commercial buildings. The site is also adjacent to the North 4th Ring Road traffic artery. It is a typical urban site and there are no industrial emissions in the vicinity. The concentrations of NO<sub>2</sub>, CO, O<sub>3</sub> and PM<sub>2.5</sub> were obtained from the Wanliu site, which is about 3 km away from the ICCAS site. The atmospheric environment of both sites was both the open area characterized as urban, so the differences in NO<sub>2</sub>, CO, O<sub>3</sub> and PM<sub>2.5</sub> concentrations of these two sites can be ignored.

### 2.2. Machine learning model-based random forest algorithm

The RF algorithm is a machine learning method based on decision trees and is capable of handling the complex non-linear response relationships between dependent and independent variables. It produces a set quantity of basic decision trees (Ntree) by utilizing resampled, randomly-selected training data with replacement. Each decision tree node is split based on the most optimal predictor from a randomly selected subset at that node (Cui and Wang, 2021). By averaging the predicted results of decision trees, the RF algorithm demonstrates reduced sensitivity to starting conditions and mitigates the overfitting problem (Geurts et al., 2006). It has been successfully applied to air quality simulations (Cui and Wang, 2021; Wen et al., 2022). Here, an ML-RF model using the RStudio software to predict hourly concentrations of HONO during the heating period, the non-heating period and the whole year. In this model, the predetermined number of Ntree is set to be 500, and the number of variables that can split at each node (mtry) is set to be 3. Seventy percent of the data is used for training and the remaining data (30%) is reserved for evaluation. The performance of the model for HONO prediction is shown in Fig. 3.

Ambient HONO has several formation pathways and its main sources include heterogeneous reaction of NO<sub>2</sub>, homogeneous reaction of NO and OH radicals, combustion emissions, photolysis of HNO<sub>3</sub> and absorbed nitrate, etc. (Spataro and Ianniello, 2014). Therefore, the level of ambient HONO is significantly influenced by the concentrations of precursors and meteorology. In this study, the input features of the model include the time variables (DOY (day of year), DOW (day of week), and hour (hour of the day)), meteorological parameters (temp, RH, WS, WD) and concentrations of pollutants (NO<sub>2</sub>, NH<sub>3</sub>, O<sub>3</sub>, SO<sub>2</sub>, CO, PM<sub>2.5</sub> and nitrate in PM<sub>2.5</sub>). The detailed list of prediction variables is given in Table 1. All variables are numerical and all have hourly resolution.

**Table 1**  
Potential prediction variables considered in HONO modelling.

Codes	Prediction variables	Units
<b>Temporal variables</b>		
DOY	Day of year, 1–365 for 365 days in a year	n/a
DOW	Day of week, 1–7 for 7 days in a week	n/a
hour	0 to 23 for 24 h in a day	n/a
<b>Meteorology</b>		
temp	Air temperature from ICCSA site	°C
RH	Relative humidity from ICCSA site	%
WS	Wind speed from ICCSA site	m s <sup>-1</sup>
WD	Wind direction from ICCSA site	degree
<b>Pollutants</b>		
NO <sub>2</sub>	From Wanliu site	ppb
NH <sub>3</sub>	From ICCSA site	ppb
O <sub>3</sub>	From Wanliu site	ppb
SO <sub>2</sub>	From ICCSA site	ppb
CO	From Wanliu site	ppm
PM <sub>2.5</sub>	From Wanliu site	µg m <sup>-3</sup>
nitrate	The concentration of nitrate in PM <sub>2.5</sub> from the ICCSA site	µg m <sup>-3</sup>

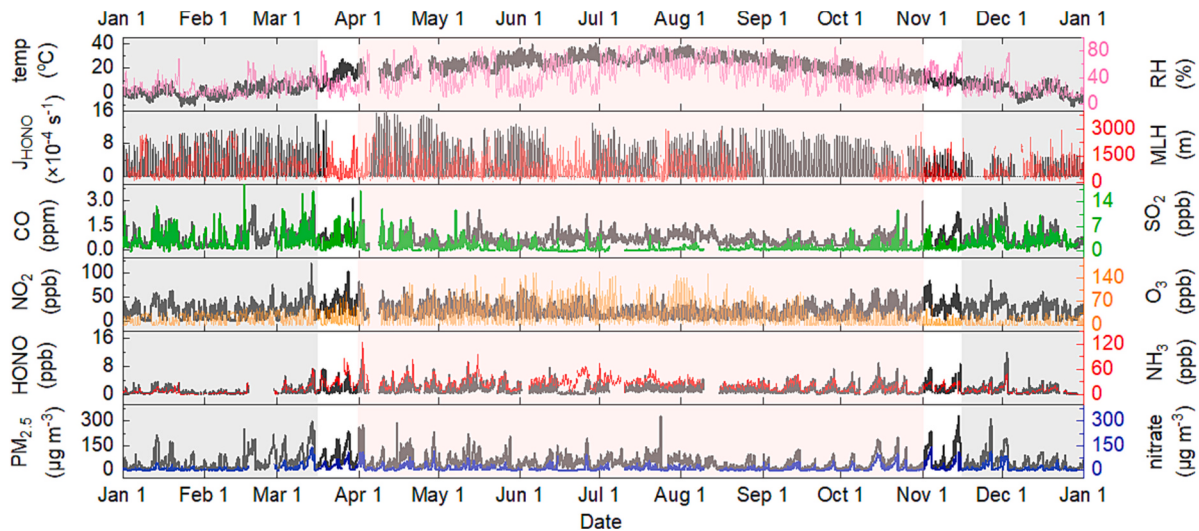
### 3. Results and discussion

#### 3.1. Overview of the measurement

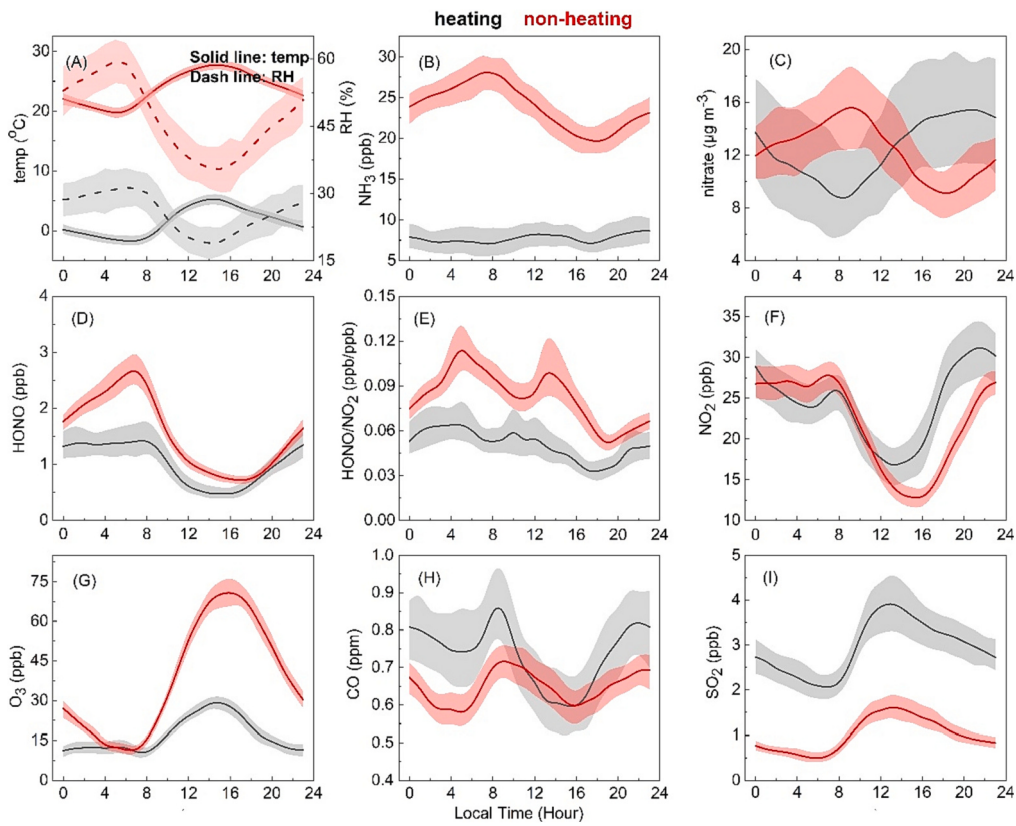
Fig. 1 shows the time series of meteorological parameters and pollutant concentrations throughout 2018. Beijing adopts natural gas central heating from November 15 to next March 15, and the data for the whole year of 2018 are divided into heating and non-heating periods. Here, January 1–March 15 and November 15–December 31 are designated as the heating period, as shown by the light grey shaded areas in Fig. 1. Meanwhile, the period from April 1 to October 31 is the non-heating period, as shown by the light red shaded area in Fig. 1. The heating period is mainly in winter and spring, and the non-heating period is mainly in summer and autumn.

Fig. 2 compares the diurnal variations of meteorological parameters and pollutants during the heating and non-heating periods. Temperature and relative humidity are significantly higher during the non-heating period than those during the heating period. The higher concentrations of CO and SO<sub>2</sub> during the heating period indicate higher combustion emissions. The daily variations of HONO are similar in both periods, HONO reaches a maximum in the morning and then

continuously decreases to a minimum in the afternoon, which is consistent with previous studies (Hu et al., 2022). The level of HONO is higher during the non-heating period than during the heating period, with mean values of  $1.54 \pm 1.32$  ppb and  $1.02 \pm 1.13$  ppb, respectively. Previous studies reported that HONO concentration is the highest during cold seasons, which is associated with higher primary emissions and lower HONO self-photolysis (Li, D. et al., 2018; Liu et al., 2019). The reasons for a higher HONO concentration during the non-heating period than that during the heating period are as follows. On the one hand, combustion emissions of HONO are lower due to lower concentrations of the primary pollutants CO and SO<sub>2</sub> (Fig. 2(H) and (I)) during the non-heating period, and the secondary formation processes of HONO could be very strong during this period. On the other hand, a series of air pollution control measures were implemented in northern China, for example, a policy “Clean Winter Heating Plan for Northern China (2017–2021)” is implemented to increase the share of clean heating in northern China (Song et al., 2023), which reduced combustion emissions of HONO during the heating period. The daily average HONO/NO<sub>2</sub> ratio is higher throughout the day in the non-heating period, suggesting more efficient HONO formation processes, such as heterogeneous conversion of NO<sub>2</sub> to HONO. Notably, in contrast to the heating period, the HONO/NO<sub>2</sub> ratio peaks around midday in the non-heating period, suggesting that strong HONO sources occur, such as light-enhanced heterogeneous reaction of NO<sub>2</sub> and/or other daytime HONO formation processes. The mean values of NO<sub>2</sub> are  $24 \pm 16$  ppb and  $22 \pm 13$  ppb during the heating and non-heating periods, respectively. The level of O<sub>3</sub> is much higher with a mean value of  $38 \pm 16$  ppb during the non-heating period due to enhanced photochemical production of O<sub>3</sub> by stronger radiation. The NH<sub>3</sub> concentration is obviously higher during the non-heating period with a diurnal mean value ranging from 19.6 ppb to 28.2 ppb while the diurnal mean value of NH<sub>3</sub> during the heating period is less than about 10 ppb. A previous study also reported that the NH<sub>3</sub> concentration is relatively higher during April–September than the other months in the urban area of Beijing (Lan et al., 2021). This could be caused by NH<sub>3</sub>-transport from agricultural fertilization areas (Gu et al., 2022) and the higher temperature during the non-heating period. The NH<sub>3</sub> concentration peaks at ~8:00 LT (Local Time, UTC + 8) and drops at ~18:00 LT during the non-heating period. The peak of NH<sub>3</sub> in the early morning could be ascribed to the evaporation of dew, resulting in the release of NH<sub>3</sub> originally stored in the droplets (Kuang et al., 2020). The diurnal variation of nitrate is similar to that of HONO during the non-heating period, implying that HONO and nitrate may have common sources (e.g. heterogeneous reaction of NO<sub>2</sub>) and/or nitrate may be the



**Fig. 1.** The time series of meteorological parameters and pollutants during 2018. Temp, RH, J<sub>HONO</sub> and MLH represent air temperature, relative humidity, photolysis frequency of HONO and mixing layer height, respectively.



**Fig. 2.** Diurnal variations of meteorological parameters and pollutants during heating and non-heating periods. Temp and RH represent air temperature and relative humidity, respectively. Black and red lines represent heating and non-heating periods, respectively. The shaded areas are the standard deviations of the parameters. (For interpretation of the references to colour in this figure legend, the reader is referred to the web version of this article.)

precursor of HONO.

In general, meteorological conditions (temperature, RH, solar radiation and wind direction), anthropogenic activities (heating and non-heating) and the levels of pollutant concentrations ( $\text{NH}_3$ ,  $\text{O}_3$ ,  $\text{SO}_2$  and  $\text{CO}$ ) are significantly different between the heating and non-heating periods, which is likely to affect the HONO chemistry in the atmosphere.

### 3.2. Performance of the ML-RF HONO models

The ML-RF models using data from the heating period, the non-heating period and the whole year are named  $M_{\text{heating}}$ ,  $M_{\text{non-heating}}$  and  $M_{\text{all}}$ , respectively. As shown in Fig. 3, all models generally perform well in predicting hourly HONO concentrations, with coefficients of determination ( $R$ ) of 0.95, 0.96, and 0.95 and with root mean square errors (RMSE) of 0.37 ppb, 0.41 ppb and 0.46 ppb, respectively. As HONO concentrations increase, the underestimation of HONO by the three models becomes significant, due to model biases in predicting extreme ranges caused by insufficient training data (Robinson et al., 2020).

The relative importance of all input variables is also output by the ML-RF models in Fig. 3. The relative importance of a particular variable is determined based on the reduction in squared error introduced by splitting of that variable in the tree-building process. A split with a large decrease is considered important, and variables used for splitting at important splits are also considered important (Wen et al., 2022). It should be noted that, relative importance can only analyze relative influences of input variables on HONO variability, but cannot determine whether the specific input variable has a positive or negative effect on HONO. During the heating period in Fig. 3 (A),  $\text{O}_3$ ,  $\text{NH}_3$ ,  $\text{RH}$ ,  $\text{WS}$  and  $\text{SO}_2$  are the five most important factors influencing ambient HONO. There are complicated reasons for the highest importance of  $\text{O}_3$ , and the main reasons are as follows. (1) Photolysis of HONO is an important source of

$\text{OH}$  radicals, which further accelerates the formation of  $\text{O}_3$  (Wang et al., 2021; Xue et al., 2021). Therefore, the importance of  $\text{O}_3$  reflects the important contribution of HONO photolysis to atmospheric oxidation capacity. (2) Tropospheric  $\text{O}_3$  is mainly produced by photochemical reactions (Li et al., 2019), so its concentration is typically high during the day and low at night, while HONO undergoes rapid self-photolysis during the day, resulting in high levels at night and low levels during the day (Zhang et al., 2020). (3) Similar to HONO,  $\text{O}_3$  is also formed from chemical reactions of  $\text{NO}_x$  ( $\text{NO}$  and  $\text{NO}_2$ ) in the troposphere. (4) It is also possible that  $\text{O}_3$  can inhibit HONO formation through heterogeneous uptake of  $\text{NO}_2$  (Han et al., 2013).  $\text{NH}_3$  ranks second in terms of variable importance. On the one hand,  $\text{NH}_3$  can be released by the combustion of fossil fuels (Pan et al., 2016), such as local vehicle exhaust, implying that HONO is closely related to primary emissions. On the other hand,  $\text{NH}_3$  concentrations can affect the aerosol liquid water content and aerosol pH, which further affect the secondary formation processes of HONO (Cheng et al., 2016; Li, L. et al., 2018; Liu and Abbatt, 2021; Zheng et al., 2020). Gaseous  $\text{SO}_2$  is a primary pollutant related to combustion emissions, and it may have common source of HONO. In addition, HONO can oxidizes  $\text{SO}_2$  to form sulfate on haze days associated with high RH in the cold winter (Wang et al., 2020), which may also lead to the high importance ranking of  $\text{SO}_2$  and  $\text{RH}$ . Based on the importance of WS, the formation of HONO may be related to primary pollutants transported from coal combustion sources in the surrounding suburban and rural areas. Moreover, wind speed also affects HONO accumulation and dispersion.

During the non-heating period in Fig. 3 (B),  $\text{NH}_3$ ,  $\text{O}_3$ , nitrate,  $\text{NO}_2$  and  $\text{RH}$  are the five most important factors. Compared to the heating period, the importance of  $\text{O}_3$  decreases from first to second. Gu et al. (2021) found that the percentage contribution of HONO photolysis to the primary formation of  $\text{OH}$  radicals in Beijing was higher in winter

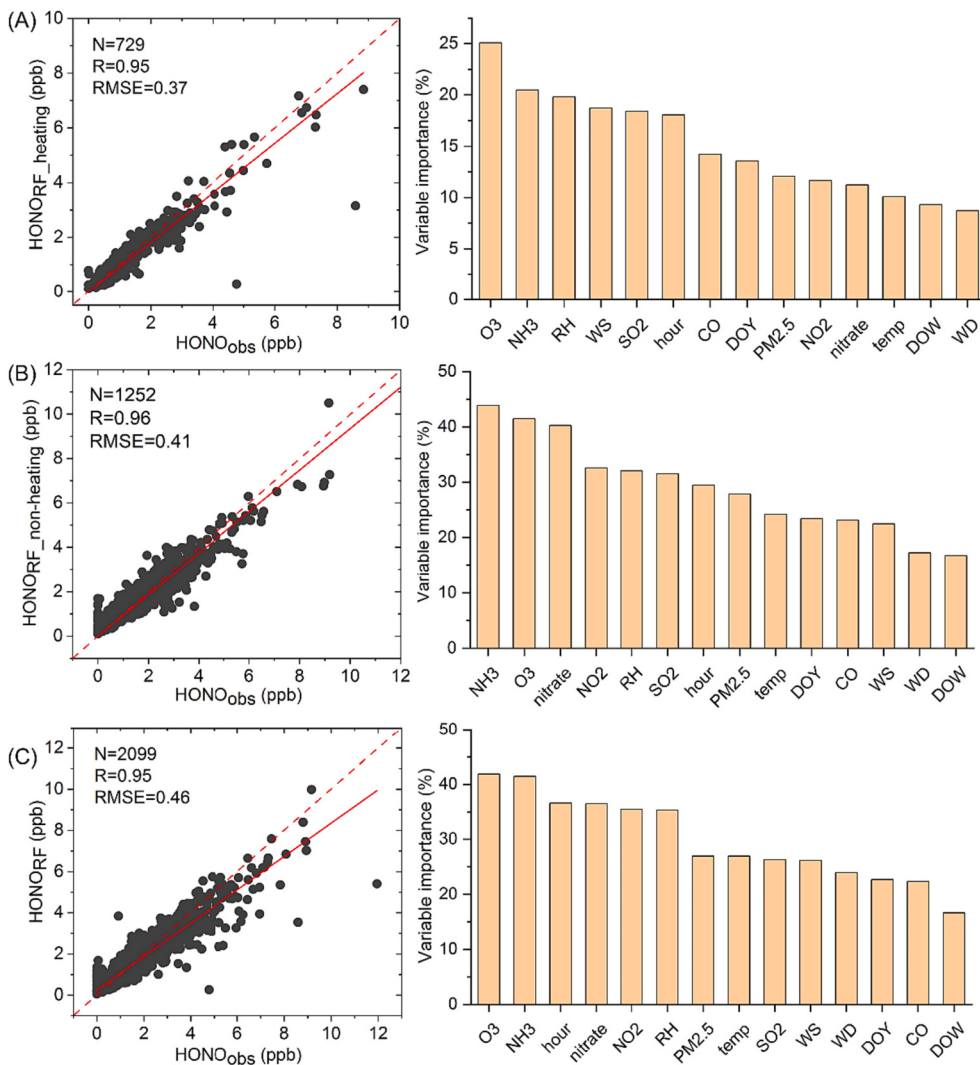


**Fig. 3.** Model performance (left) and variable importance (right) for ambient HONO in 2018. Prediction results of (A), (B) and (C) are from ML-RF HONO models  $M_{\text{heating}}$ ,  $M_{\text{non-heating}}$  and  $M_{\text{all}}$ , respectively. Linear fits between predicted and observed data are indicated by red solid lines, and red dashed lines are the ideal 1:1 lines. (For interpretation of the references to colour in this figure legend, the reader is referred to the web version of this article.)

than in summer. Aumont et al. (2003) found that HONO sources were the major contributors to the primary production of OH radicals, leading to larger changes in O<sub>3</sub> and HO<sub>x</sub> levels in winter than in summer. These results show a more important influence of HONO on the atmospheric oxidation capacity during the heating season (Eshorbany et al., 2012). RH is much higher with daily mean values ranging in 35–59% during the non-heating period as shown in Fig. 2 (A). Previous studies reported that higher RH can promote NO<sub>2</sub> heterogeneous reaction to produce HONO when RH is less than about 70% (Li et al., 2012; Yu et al., 2009). Therefore, the prominent importance of NO<sub>2</sub> during the non-heating period is attributed to the higher RH. Our previous study also reported that the heterogeneous reaction of NO<sub>2</sub> is the dominant source of HONO in the urban area of Beijing in spring 2018 (Zhang et al., 2020). In addition, due to more precipitation processes in the non-heating period, RH may affect the wet deposition of ambient HONO. Cui and Wang (2021) also reported the importance of RH for the spatio-temporal variability of HONO. Notably, the high importance of nitrate is found during the non-heating period. It is mainly attributed to (1) nitrate and HONO are both generated from the important heterogeneous reaction of NO<sub>2</sub> during this period (2) the photolysis of absorbed nitrate may be a more critical source of HONO in the non-heating period with strong radiation than that in the heating period (Andersen et al., 2023; Cui and Wang, 2021; Ye et al., 2017). Furthermore, NH<sub>3</sub> shows the highest

importance in this period. Although NH<sub>3</sub> could promote the heterogeneous reaction of NO<sub>2</sub> to form HONO (Li et al., 2018a, 2018b; Wang et al., 2016; Xu et al., 2019), the importance of NH<sub>3</sub> exceeds that of NO<sub>2</sub> and RH, suggesting that in addition to the role of NH<sub>3</sub> in the conversion of NO<sub>2</sub> to HONO, there must be other close relationships between NH<sub>3</sub> and HONO in the atmosphere. Kebede et al. (2013) reported that irradiation of TiO<sub>2</sub> in the presence of NH<sub>3</sub> releases HONO under atmospheric conditions. Therefore, NH<sub>3</sub> may be an important precursor of HONO, which should be further investigated. Based on the close relationship between NH<sub>3</sub> and HONO as discussed above, the significantly higher concentration of NH<sub>3</sub> (shown in Section 3.1) during this period may enhance the effect of NH<sub>3</sub> on HONO.

For the entire 2018 measurement in Fig. 3 (C), the top five factors are O<sub>3</sub>, NH<sub>3</sub>, hour, nitrate and NO<sub>2</sub>. The factors O<sub>3</sub>, NH<sub>3</sub>, nitrate and NO<sub>2</sub> are closely related to the chemical formation mechanisms of HONO, as discussed above during the heating and non-heating periods. The importance of hour suggests that HONO concentrations suffered from more significant daily variations because HONO undergoes rapid self-photolysis during the day and accumulates at night. In addition, meteorological variables (RH, WS, temp and WD) also showed some importance due to their influence on HONO formation mechanisms, (wet and dry) deposition and diffusion.

### 3.3. Impact of meteorology on HONO

Based on the influence of meteorological variables on ambient HONO, a weather normalization process is performed to eliminate the influence of meteorological variables on the HONO concentration during the heating and non-heating periods. Fig. 4 shows the variation of HONO with temperature, RH, WS and WD. HONO levels are highest in the 10–20 °C temperature range. In addition, HONO concentration increases with RH when RH is less than ~70%, and HONO decreases with increasing RH when RH is greater than ~70%. Based on the importance of NO<sub>2</sub> to HONO in Fig. 3 (C), the relationships between HONO and temperature, relative humidity may be due to the influence of these two meteorological variables on the generation of HONO from NO<sub>2</sub> heterogeneous reaction. Our previous study found that NO<sub>2</sub> heterogeneous conversion to HONO has an optimal temperature (~10 °C) (Zhang et al., 2023), which is roughly consistent with the temperature corresponding to the highest level of HONO in Fig. 4 (A). In addition, relative humidity is widely considered to be an important influencing factor in the conversion of NO<sub>2</sub> to HONO, which could promote HONO formation at RH < ~70% and not be conducive to HONO formation at RH > ~70% (Li et al., 2012). The HONO concentration increases with the lower wind speed. In addition, the higher HONO concentration corresponds to the southeast wind, while the lower HONO concentration corresponds to the northwest wind direction. This is because the north-west of Beijing is mainly mountainous, where there are few anthropogenic emissions, while the south-east of Beijing includes Tianjin, Hebei and Shandong provinces, where there are intensive anthropogenic emissions. Therefore, the northwest wind tends to carry clean air masses and the southwest wind tends to carry polluted air masses. Wind speed and wind direction are the main factors influencing HONO dispersion.

As meteorological variables have an important influence on the HONO concentration, the weather normalization for HONO is performed based on the ML-RF algorithm. Specifically, the real-time meteorological parameters are replaced by the diurnal patterns of meteorological parameters in the ML-RF model M<sub>all</sub> throughout the year to obtain predicted HONO concentrations (denoted HONO<sub>pre</sub>). As can be

seen in Fig. 5, when considering the predicted HONO concentration, the level of HONO during the non-heating period is still higher than that during the heating period. However, the discrepancy of the predicted HONO concentrations between two periods is  $0.33 \pm 0.30$  ppb, which is smaller than that of the observed HONO concentrations ( $0.52 \pm 0.37$  ppb), indicating the non-negligible importance of meteorology in regulating HONO levels.

### 3.4. Validating the transferability of HONO estimates by ML-RF models

To assess the performance of the ML-RF algorithm in predicting HONO in other years, we further compare the learning predictions of the ML-RF HONO model with observations for each of the three periods in Beijing. These three periods are carefully selected: May 21–June 21 in 2017 (P1), December 15–31 in 2017 (P2) and March 1–15 in 2021 (P3), respectively. P1 is the non-heating period close to 2018, P2 is the heating period closest to 2018, and P3 is the heating period far from 2018. The model M<sub>non-heating</sub> is used to predict HONO for P1, and the model M<sub>heating</sub> is used to predict HONO for P2 and P3. The relationships between prediction results and observed HONO are shown in Fig. 6. The ML-RF models based on 2018 data are able to roughly predict HONO for three periods in 2017 and 2021 with R values in P1, P2 and P3 of 0.76, 0.87 and 0.89, respectively, and RMSE values of 0.71 ppb, 0.74 ppb and 1.08 ppb, respectively. Furthermore, the biases between observed HONO (HONO<sub>obs</sub>) and predicted HONO (HONO<sub>RF</sub>) in P1, P2 and P3 are derived (bias = HONO<sub>RF</sub> - HONO<sub>obs</sub>), and the ML-RF algorithm is used to explore the main independent variables (shown in Table 1) related to the bias between HONO<sub>obs</sub> and HONO<sub>RF</sub>. The predicted HONO biases (bias<sub>RF</sub>) for P1, P2 and P3 by the ML-RF algorithm are shown in Fig. 7, the agreement between bias and bias<sub>RF</sub> is roughly good, with the R values of 0.86, 0.85 and 0.74 for P1, P2 and P3, respectively. The variable importance output by the ML-RF model is the potential driving factors of the biases between HONO<sub>obs</sub> and HONO<sub>RF</sub> for P1, P2 and P3, and the higher rank in the variable importance indicates the greater influence of that feature on the target learning value.

In Fig. 6 (A), the prediction underestimates HONO when HONO

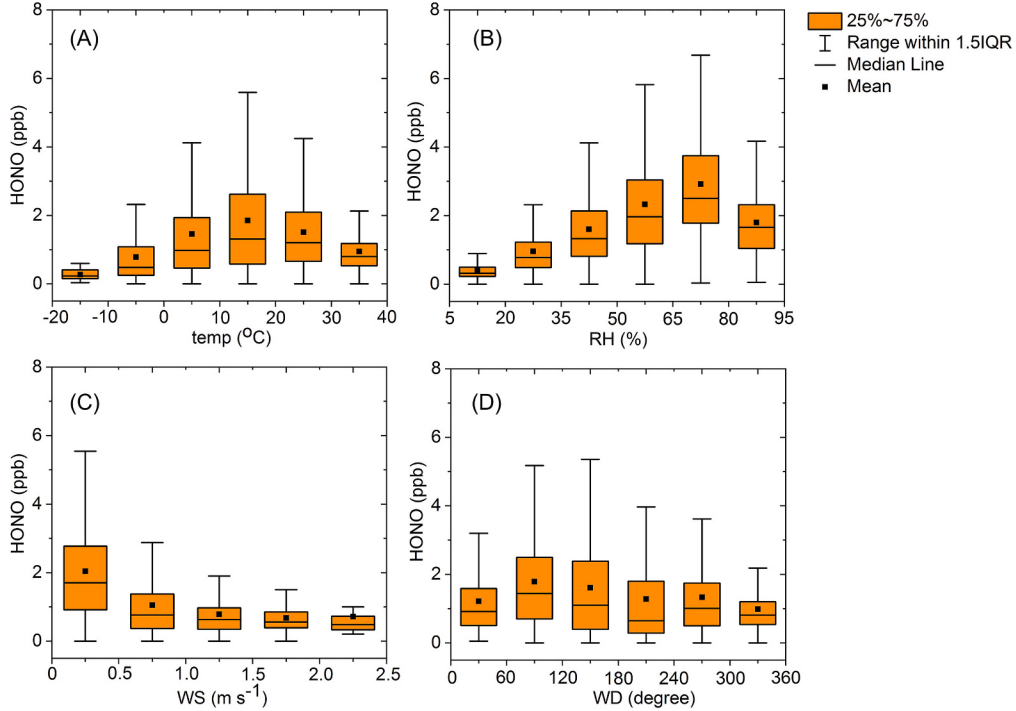


**Fig. 4.** The relationships between observed HONO concentrations and temperature (temp), relative humidity (RH), wind speed (WS) and wind direction (WD) in 2018.

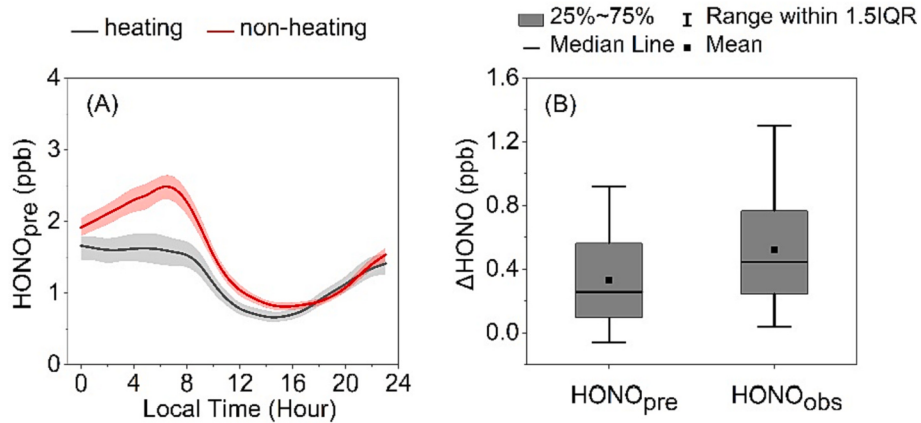


**Fig. 5.** (A) The diurnal variations of predicted HONO during heating and non-heating periods. The shaded areas are the standard deviations of HONO<sub>pre</sub>. (B) Box charts of the discrepancies of HONO concentrations ( $\Delta\text{HONO}$ ) between heating and non-heating periods. HONO<sub>pre</sub> and HONO<sub>obs</sub> represent the predicted and observed HONO, respectively.

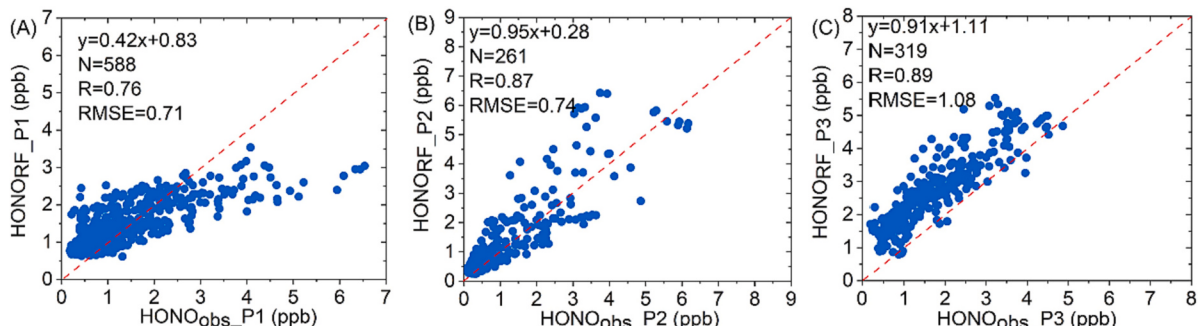


**Fig. 6.** Model performance for HONO in May 21–June 21 in 2017 (P1), December 15–31 in 2017 (P2) and March 1–15 in 2021 (P3). HONO<sub>RF</sub> and HONO<sub>obs</sub> are the predicted HONO by the ML-RF HONO models and the observed HONO, respectively. Red dashed lines are the ideal 1:1 lines. (For interpretation of the references to colour in this figure legend, the reader is referred to the web version of this article.)

concentrations are more than  $\sim 3$  ppb in P1, in other words, the predicted values obtained under the constraint of pollutants (independent variables) in the model cannot reach the level of HONO in the atmosphere. This could mean that the chemical generation processes of HONO are stronger in P1, compared to the non-heating period of 2018. Moreover, based on the prominent importance of NO<sub>2</sub> and RH in Fig. 7 (A), the stronger chemical generation processes of HONO in P1 might be related to NO<sub>2</sub> heterogeneous reaction. P2 is related to the heating period in 2018, and the best predicted results are found compared to P1 and P3 as seen in Fig. 6. For P2, NO<sub>2</sub>, PM<sub>2.5</sub> and NH<sub>3</sub> have a large impact on the bias (Fig. 7 (B)), because PM<sub>2.5</sub> and NH<sub>3</sub> could be significant factors influencing the heterogeneous conversion of NO<sub>2</sub> to HONO (Hou et al., 2016; Xu et al., 2019). The overestimation of the prediction in P3 in Fig. 6 (C) can be attributed to the different dispersion conditions and primary emissions between 2021 and 2018, according to the prominent importance of CO and WS for the bias in Fig. 7 (C). Section 3.2 In summary, the ML-RF models based on 2018 data are able to roughly predict HONO for three periods in 2017 and 2021, although there are still biases between predicted and observed values due to differences in the secondary formation of HONO in the non-heating period (P1) and the effects of primary emissions and meteorological factors in the heating period (P3).

#### 4. Conclusion

In this study, machine learning is used to investigate the main factors affecting HONO chemistry during the heating and non-heating periods in Beijing in 2018. The ML-RF models show satisfactory performance

during the heating and non-heating periods and throughout the year. Primary emissions and diffusion have obvious impacts on ambient HONO during the heating period, while chemical formation processes such as NO<sub>2</sub> heterogeneous reaction and nitrate photolysis are important for HONO during the non-heating period. O<sub>3</sub> and NH<sub>3</sub> are the most important variables for HONO during both periods, which may indicate the close link between HONO and atmospheric oxidation and the important role of NH<sub>3</sub> in HONO formation processes. Overall, due to the differences in meteorological conditions and pollutant emission characteristics between the heating and non-heating periods, the main influencing factors of HONO are different. Therefore, the parameterization scheme for HONO in chemical models should be cautious during different periods when meteorological conditions and pollutant emission characteristics vary greatly. In addition, the ML-RF models based on 2018 data are able to roughly predict HONO for three periods in 2017 and 2021. The biases between observed and predicted HONO in P1 are mainly related to differences in secondary formation processes of HONO (such as heterogeneous reaction of NO<sub>2</sub>) between 2017 and 2018. The overestimation of the prediction in P3 can be attributed to different dispersion conditions and/or primary emissions between 2021 and 2018. In the future, the prediction of HONO will be improved with sufficient training data in the ML model, especially for high and low concentrations of HONO across years. This study suggests that machine learning methods using limited meteorological and pollutant parameters can offer great advantages in predicting HONO concentrations. At the same time, machine learning can also provide some hints for the chemical model parameterization scheme, for example, it can find the variables closely related to ambient HONO through a large amount of

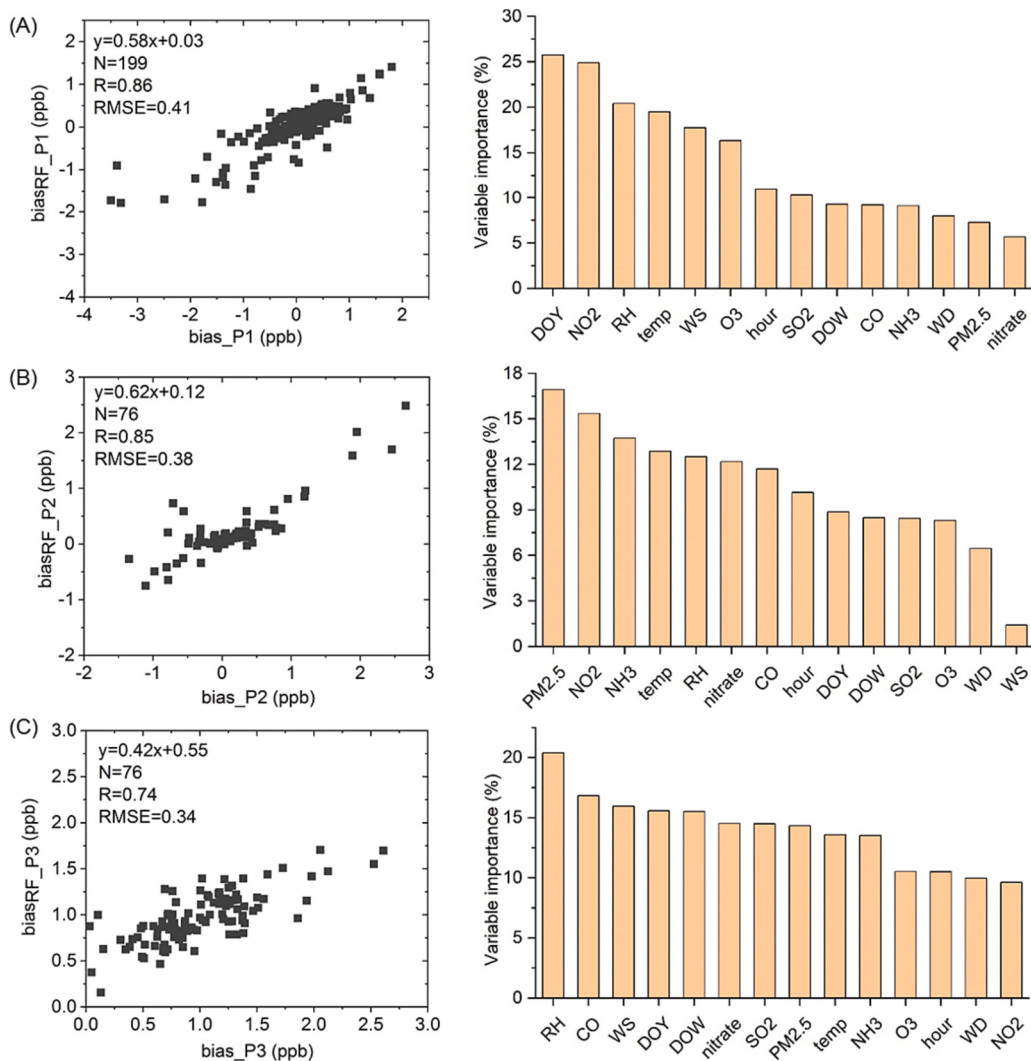


**Fig. 7.** Scatter plots of biases (bias = HONO<sub>RF</sub>-HONO<sub>obs</sub>) and RF-predicted biases (bias<sub>RF</sub>) by the ML-RF model for P1 (A), P2 (B) and P3 (C). And the corresponding variable importance for biases in P1, P2 and P3 is shown on the right.

data, which can further improve the chemical mechanisms of HONO.

#### CRediT authorship contribution statement

**Wenqian Zhang:** Conceptualization, Data curation, Formal analysis, Funding acquisition, Investigation, Methodology, Software, Writing – original draft. **Shengrui Tong:** Conceptualization, Data curation, Formal analysis, Funding acquisition, Methodology, Writing – review & editing. **Siqi Hou:** Conceptualization, Formal analysis, Software. **Pusheng Zhao:** Data curation, Investigation. **Yuepeng Pan:** Data curation, Investigation. **Lili Wang:** Data curation, Investigation. **Mengtian Cheng:** Data curation, Investigation. **Dongsheng Ji:** Data curation, Investigation. **Guqian Tang:** Data curation, Investigation. **Bo Hu:** Data curation, Investigation. **Xin Li:** Data curation, Investigation. **Maofa Ge:** Funding acquisition, Supervision, Writing – review & editing.

#### Declaration of Competing Interest

The authors declare that they have no known competing financial interests or personal relationships that could have appeared to influence the work reported in this paper.

#### Data availability

Data will be made available on request.

#### Acknowledgements

This work was supported by National Natural Science Foundation of China (Nos. 42022039, 41830106), Beijing National Laboratory for Molecular Sciences (No. BNLMS-CXXM-202011), Youth Innovation Promotion Association of Chinese Academy of Sciences (No. Y2021013), China Postdoctoral Science Foundation (No. 2022M713199).

#### References

- Andersen, S.T., Carpenter, L.J., Reed, C., Lee, J.D., Chance, R., Sherwen, T., Vaughan, A.R., Stewart, J., Edwards, P.M., Bloss, W.J., Sommariva, R., Crilley, L.R., Nott, G.J., Neves, L., Read, K., Heard, D.E., Seakins, P.W., Whalley, L.K., Boustead, G.A., Fleming, L.T., Stone, D., Fomba, K.W., 2023. Extensive field evidence for the release of HONO from the photolysis of nitrate aerosols. Sci. Adv. 9, eadd6266. <https://doi.org/10.1126/sciadv.add6266>.
- Aumont, B., Chervier, F., Laval, S., 2003. Contribution of HONO sources to the NO<sub>x</sub>/HO<sub>x</sub>/O<sub>3</sub> chemistry in the polluted boundary layer. Atmos. Environ. 37 [https://doi.org/10.1016/s1352-2310\(02\)00920-2](https://doi.org/10.1016/s1352-2310(02)00920-2). pii s1352-2310(02)00920-2. 487-498.
- Chai, J., Dibb, J.E., Anderson, B.E., Bekker, C., Blum, D.E., Heim, E., Jordan, C.E., Joyce, E.E., Kaspari, J.H., Munro, H., Walters, W.W., Hastings, M.G., 2021. Isotopic evidence for dominant secondary production of HONO in near-ground wildfire

- plumes. *Atmos. Chem. Phys.* 21, 13077–13098. <https://doi.org/10.5194/acp-21-13077-2021>.
- Chen, X., Walker, J.T., Geron, C., 2017. Chromatography related performance of the Monitor for AeRosols and GAses in ambient air (MARGA): laboratory and field-based evaluation. *Atmos. Meas. Tech.* 10, 3893–3908. <https://doi.org/10.5194/amt-10-3893-2017>.
- Cheng, Y.F., Zheng, G.J., Wei, C., Mu, Q., Zheng, B., Wang, Z.B., Gao, M., Zhang, Q., He, K.B., Carmichael, G., Poschl, U., Su, H., 2016. Reactive nitrogen chemistry in aerosol water as a source of sulfate during haze events in China. *Sci. Adv.* 2 <https://doi.org/10.1126/sciadv.1601530>.
- Cui, L., Wang, S., 2021. Mapping the daily nitrous acid (HONO) concentrations across China during 2006–2017 through ensemble machine-learning algorithm. *Sci. Total Environ.* 785, 147325. <https://doi.org/10.1016/j.scitotenv.2021.147325>.
- Ding, X., Huang, C., Liu, W., Ma, D., Lou, S., Li, Q., Chen, J., Yang, H., Xue, C., Cheng, Y., Su, H., 2023. Direct observation of HONO emissions from real-world residential natural gas heating in China. *Environ. Sci. Technol.* <https://doi.org/10.1021/acs.est.2c09386>.
- Elshorbany, Y.F., Kleffmann, J., Kurtenbach, R., Lissi, E., Rubio, M., Villena, G., Gramsch, E., Rickard, A.R., Pilling, M.J., Wiesen, P., 2010. Seasonal dependence of the oxidation capacity of the city of Santiago de Chile. *Atmos. Environ.* 44, 5383–5394. <https://doi.org/10.1016/j.atmosenv.2009.08.036>.
- Elshorbany, Y.F., Steil, B., Bruhl, C., Lelieveld, J., 2012. Impact of HONO on global atmospheric chemistry calculated with an empirical parameterization in the EMAC model. *Atmos. Chem. Phys.* 12, 9977–10000. <https://doi.org/10.5194/acp-12-9977-2012>.
- Geurts, P., Ernst, D., Wehenkel, L., 2006. Extremely randomized trees. *Mach. Learn.* 63, 3–42. <https://doi.org/10.1007/s10994-006-6226-1>.
- Grange, S.K., Carslaw, D.C., Lewis, A.C., Boleti, E., Hueglin, C., 2018. Random forest meteorological normalization models for Swiss PM<sub>10</sub> trend analysis. *Atmos. Chem. Phys.* 18, 6223–6239. <https://doi.org/10.5194/acp-18-6223-2018>.
- Gu, R., Shen, H., Xue, L., Wang, T., Gao, J., Li, H., Liang, Y., Xia, M., Yu, C., Liu, Y., Wang, W., 2021. Investigating the sources of atmospheric nitrous acid (HONO) in the megacity of Beijing, China. *Sci. Total Environ.* 152270. <https://doi.org/10.1016/j.scitotenv.2021.152270>.
- Gu, M., Pan, Y., Sun, Q., Walters, W.W., Song, L., Fang, Y., 2022. Is fertilization the dominant source of ammonia in the urban atmosphere? *Sci. Total Environ.* 838, 155890. <https://doi.org/10.1016/j.scitotenv.2022.155890>.
- Han, C., Liu, Y., He, H., 2013. Role of organic carbon in heterogeneous reaction of NO<sub>2</sub> with soot. *Environ. Sci. Technol.* 47, 3174–3181. <https://doi.org/10.1021/es304468n>.
- Hou, S.Q., Tong, S.R., Ge, M.F., An, J.L., 2016. Comparison of atmospheric nitrous acid during severe haze and clean periods in Beijing, China. *Atmos. Environ.* 124, 199–206. <https://doi.org/10.1016/j.atmosenv.2015.06.023>.
- Hu, B., Duan, J., Hong, Y., Xu, L., Li, M., Bian, Y., Qin, M., Fang, W., Xie, P., Chen, J., 2022. Exploration of the atmospheric chemistry of nitrous acid in a coastal city of southeastern China: results from measurements across four seasons. *Atmos. Chem. Phys.* 22, 371–393. <https://doi.org/10.5194/acp-22-371-2022>.
- Kebede, M.A., Scharko, N.K., Appelt, L.E., Raff, J.D., 2013. Formation of nitrous acid during ammonia photooxidation on TiO<sub>2</sub> under atmospherically relevant conditions. *J. Phys. Chem. Lett.* 4, 2618–2623. <https://doi.org/10.1021/jz401250k>.
- Kim, S., VandenBoer, T.C., Young, C.J., Riedel, T.P., Thornton, J.A., Swarthout, B., Sive, B., Lerner, B., Gilman, J.B., Warneke, C., Roberts, J.M., Guenther, A., Wagner, N.L., Dube, W.P., Williams, E., Brown, S.S., 2014. The primary and recycling sources of OH during the NACHTT-2011 campaign: HONO as an important OH primary source in the wintertime. *J. Geophys. Res.* 119, 6886–6896. <https://doi.org/10.1002/2013jd019784>.
- Kleffmann, J., 2007. Daytime sources of nitrous acid (HONO) in the atmospheric boundary layer. *Chemphyschem*, 8, 1137–1144. <https://doi.org/10.1002/cphc.200700016>.
- Kuang, Y., Xu, W., Lin, W., Meng, Z., Zhao, H., Ren, S., Zhang, G., Liang, L., Xu, X., 2020. Explosive morning growth phenomena of NH<sub>3</sub> on the North China Plain: causes and potential impacts on aerosol formation. *Environ. Pollut.* 257, 113621. <https://doi.org/10.1016/j.envpol.2019.113621>.
- Lan, Z., Lin, W., Pu, W., Ma, Z., 2021. Measurement report: exploring NH<sub>3</sub> behavior in urban and suburban Beijing: comparison and implications. *Atmos. Chem. Phys.* 21, 4561–4573. <https://doi.org/10.5194/acp-21-4561-2021>.
- Li, X., Brauers, T., Haeseler, R., Bohn, B., Fuchs, H., Hofzumahaus, A., Holland, F., Lou, S., Lu, K.D., Rohrer, F., Hu, M., Zeng, L.M., Zhang, Y.H., Garland, R.M., Su, H., Nowak, A., Wiedensohler, A., Takegawa, N., Shao, M., Wahner, A., 2012. Exploring the atmospheric chemistry of nitrous acid (HONO) at a rural site in Southern China. *Atmos. Chem. Phys.* 12, 1497–1513. <https://doi.org/10.5194/acp-12-1497-2012>.
- Li, L., Duan, Z., Li, H., Zhu, C., Henkelman, G., Francisco, J.S., Zeng, X.C., 2018a. Formation of HONO from the NH<sub>3</sub>-promoted hydrolysis of NO<sub>2</sub> dimers in the atmosphere. *Proc. Natl. Acad. Sci. U. S. A.* 115, 7236–7241. <https://doi.org/10.1073/pnas.1807719115>.
- Li, D., Xue, L., Wen, L., Wang, X., Chen, T., Mellouki, A., Chen, J., Wang, W., 2018b. Characteristics and sources of nitrous acid in an urban atmosphere of northern China: results from 1-yr continuous observations. *Atmos. Environ.* 182, 296–306. <https://doi.org/10.1016/j.atmosenv.2018.03.033>.
- Li, K., Jacob, D.J., Liao, H., Zhu, J., Shah, V., Shen, L., Bates, K.H., Zhang, Q., Zhai, S., 2019. A two-pollutant strategy for improving ozone and particulate air quality in China. *Nat. Geosci.* 12, 906–910. <https://doi.org/10.1038/s41561-019-0464-x>.
- Li, R., Cui, L.L., Zhao, Y.L., Zhou, W.H., Fu, H.B., 2021. Long-term trends of ambient nitrate (NO<sub>3</sub>) concentrations across China based on ensemble machine-learning models. *Earth Syst. Sci. Data.* 13, 2147–2163. <https://doi.org/10.5194/essd-13-2147-2021>.
- Liang, M., Tao, J., Ma, N., Kuang, Y., Zhang, Y., Wu, S., Jiang, X., He, Y., Chen, C., Yang, W., Zhou, Y., Cheng, P., Xu, W., Hong, J., Wang, Q., Zhao, C., Zhou, G., Sun, Y., Zhang, Q., Su, H., Cheng, Y., 2022. Prediction of CCN spectra parameters in the North China Plain using a random forest model. *Atmos. Environ.* 289, 119323. <https://doi.org/10.1016/j.atmosenv.2022.119323>.
- Liao, S., Zhang, J., Yu, F., Zhu, M., Liu, J., Ou, J., Dong, H., Sha, Q., Zhong, Z., Xie, Y., Luo, H., Zhang, L., Zheng, J., 2021. High gaseous nitrous acid (HONO) emissions from light-duty diesel vehicles. *Environ. Sci. Technol.* 55, 200–208. <https://doi.org/10.1021/acs.est.0c05599>.
- Liu, T., Abbatt, J.P.D., 2021. Oxidation of sulfur dioxide by nitrogen dioxide accelerated at the interface of deliquescent aerosol particles. *Nat. Chem.* 13, 1173–1177. <https://doi.org/10.1038/s41557-021-00777-0>.
- Liu, Z., Wang, Y., Costabile, F., Amoroso, A., Zhao, C., Huey, L.G., Stickel, R., Liao, J., Zhu, T., 2014. Evidence of aerosols as a media for rapid daytime HONO production over China. *Environ. Sci. Technol.* 48, 14386–14391. <https://doi.org/10.1021/es504163z>.
- Liu, Y., Nie, W., Xu, Z., Wang, T., Wang, R., Li, Y., Wang, L., Chi, X., Ding, A., 2019. Semi-quantitative understanding of source contribution to nitrous acid (HONO) based on 1 year of continuous observation at the SORPES station in eastern China. *Atmos. Chem. Phys.* 19, 13289–13308. <https://doi.org/10.5194/acp-19-13289-2019>.
- Ma, X., Tan, Z., Lu, K., Yang, X., Liu, Y., Li, S., Li, X., Chen, S., Novelli, A., Cho, C., Zeng, L., Wahner, A., Zhang, Y., 2019. Winter photochemistry in Beijing: observation and model simulation of OH and HO<sub>2</sub> radicals at an urban site. *Sci. Total Environ.* 685, 85–95. <https://doi.org/10.1016/j.scitotenv.2019.05.329>.
- Pan, Y., Tian, S., Liu, D., Fang, Y., Zhu, X., Zhang, Q., Zheng, B., Michalski, G., Wang, Y., 2016. Fossil fuel combustion-related emissions dominate atmospheric ammonia sources during severe haze episodes: evidence from <sup>15</sup>N-stable isotope in size-resolved aerosol ammonium. *Environ. Sci. Technol.* 50, 8049–8056. <https://doi.org/10.1021/acs.est.6b00634>.
- Philibert, A., Loyce, C., Makowski, D., 2013. Prediction of N<sub>2</sub>O emission from local information with Random Forest. *Environ. Pollut.* 177, 156–163. <https://doi.org/10.1016/j.envpol.2013.02.019>.
- Robinson, M.C., Glen, R.C., Lee, A.A., 2020. Validating the validation: reanalyzing a large-scale comparison of deep learning and machine learning models for bioactivity prediction. *J. Comput. Aid. Mol. Des.* 34, 717–730. <https://doi.org/10.1007/s10822-019-00274-0>.
- Rumsey, I.C., Cowen, K.A., Walker, J.T., Kelly, T.J., Hanft, E.A., Mishoe, K., Rogers, C., Proost, R., Beachley, G.M., Lear, G., Frelink, T., Otjes, R.P., 2014. An assessment of the performance of the Monitor for AeRosols and GAses in ambient air (MARGA): a semi-continuous method for soluble compounds. *Atmos. Chem. Phys.* 14, 5639–5658. <https://doi.org/10.5194/acp-14-5639-2014>.
- Shi, Z., Song, C., Liu, B., Lu, G., Xu, J., Van Vu, T., Elliott, R.J.R., Li, W., Bloss, W.J., Harrison, R.M., 2021. Abrupt but smaller than expected changes in surface air quality attributable to COVID-19 lockdowns. *Sci. Adv.* 7 <https://doi.org/10.1126/sciadv.abd6696>.
- Song, C., Liu, B., Cheng, K., Cole, M.A., Dai, Q., Elliott, R.J.R., Shi, Z., 2023. Attribution of air quality benefits to clean winter heating policies in China: combining machine learning with causal inference. *Environ. Sci. Technol.* <https://doi.org/10.1021/acs.est.2c06800>.
- Spataro, F., Ianniello, A., 2014. Sources of atmospheric nitrous acid: state of the science, current research needs, and future prospects. *J. Air Waste Manage. Assoc.* 64, 1232–1250. <https://doi.org/10.1080/10962247.2014.952846>.
- Stieger, B., Spindler, G., Fahrlbusch, B., Müller, K., Grüner, A., Poulaïn, L., Thöni, L., Seitzer, E., Wallasch, M., Herrmann, H., 2017. Measurements of PM<sub>10</sub> ions and trace gases with the online system MARGA at the research station Melpitz in Germany – a five-year study. *J. Atmos. Chem.* 75, 33–70. <https://doi.org/10.1007/s10874-017-9361-0>.
- Stutz, J., Aliche, B., Ackermann, R., Geyer, A., Wang, S.H., White, A.B., Williams, E.J., Spicer, C.W., Fast, J.D., 2004. Relative humidity dependence of HONO chemistry in urban areas. *J. Geophys. Res.* 109 (D03307), 1–12. <https://doi.org/10.1029/2003jd004135>.
- Su, J., Zhao, P., Ge, S., Ding, J., 2022. Aerosol liquid water content of PM<sub>2.5</sub> and its influencing factors in Beijing, China. *Sci. Total Environ.* 839, 156342. <https://doi.org/10.1016/j.scitotenv.2022.156342>.
- Wang, X., Bai, F.Y., Sun, Y.Q., Wang, R.S., Pan, X.M., Tao, F.M., 2016. Theoretical study of the gaseous hydrolysis of NO<sub>2</sub> in the presence of NH<sub>3</sub> as a source of atmospheric HONO. *Environ. Chem.* 13, 611. <https://doi.org/10.1071/en15076>.
- Wang, J., Li, J., Ye, J., Zhao, J., Wu, Y., Hu, J., Liu, D., Nie, D., Shen, F., Huang, X., Huang, D.D., Ji, D., Sun, X., Xu, W., Guo, J., Song, S., Qin, Y., Liu, P., Turner, J.R., Lee, H.C., Hwang, S., Liao, H., Martin, S.T., Zhang, Q., Chen, M., Sun, Y., Ge, X., Jacob, D.J., 2020. Fast sulfate formation from oxidation of SO<sub>2</sub> by NO<sub>2</sub> and HONO observed in Beijing haze. *Nat. Commun.* 11, 2844. <https://doi.org/10.1038/s41467-020-16683-x>.
- Wang, Y., Fu, X., Wu, D., Wang, M., Lu, K., Mu, Y., Liu, Z., Zhang, Y., Wang, T., 2021. Agricultural fertilization aggravates air pollution by stimulating soil nitrous acid emissions at high soil moisture. *Environ. Sci. Technol.* 55, 14556–14566. <https://doi.org/10.1021/acs.est.1c04134>.
- Wen, Y., Zhou, Z., Zhang, S., Wallington, T.J., Shen, W., Tan, Q., Deng, Y., Wu, Y., 2022. Urban-rural disparities in air quality responses to traffic changes in a megacity of China revealed using machine learning. *Environ. Sci. Technol. Lett.* 9, 592–598. <https://doi.org/10.1021/acs.estlett.2c00246>.
- Xu, W., Kuang, Y., Zhao, C., Tao, J., Zhao, G., Bian, Y., Yang, W., Yu, Y., Shen, C., Liang, L., Zhang, G., Lin, W., Xu, X., 2019. NH<sub>3</sub>-promoted hydrolysis of NO<sub>2</sub> induces explosive growth in HONO. *Atmos. Chem. Phys.* 19, 10557–10570. <https://doi.org/10.5194/acp-19-10557-2019>.

- Xue, C., Ye, C., Zhang, C., Catoire, V., Liu, P., Gu, R., Zhang, J., Ma, Z., Zhao, X., Zhang, W., Ren, Y., Krysztófiak, G., Tong, S., Xue, L., An, J., Ge, M., Mellouki, A., Mu, Y., 2021. Evidence for strong HONO emission from fertilized agricultural fields and its remarkable impact on regional O<sub>3</sub> pollution in the summer North China Plain. *ACS Earth Space Chem.* 5, 340–347. <https://doi.org/10.1021/acsearthspacechem.0c00314>.
- Xue, C., Ye, C., Kleffmann, J., Zhang, W., He, X., Liu, P., Zhang, C., Zhao, X., Liu, C., Ma, Z., Liu, J., Wang, J., Lu, K., Catoire, V., Mellouki, A., Mu, Y., 2022. Atmospheric measurements at Mt. Tai – Part II: HONO budget and radical (RO<sub>x</sub>+NO<sub>3</sub>) chemistry in the lower boundary layer. *Atmos. Chem. Phys.* 22, 1035–1057. <https://doi.org/10.5194/acp-2021-531>.
- Ye, C., Zhang, N., Gao, H., Zhou, X., 2017. Photolysis of particulate nitrate as a source of HONO and NO<sub>x</sub>. *Environ. Sci. Technol.* 51, 6849–6856. <https://doi.org/10.1021/acs.est.7b00387>.
- Ye, X., Wang, X., Zhang, L., 2022. Diagnosing the model bias in simulating daily surface ozone variability using a machine learning method: the effects of dry deposition and cloud optical depth. *Environ. Sci. Technol.* 56, 16665–16675. <https://doi.org/10.1021/acs.est.2c05712>.
- Yu, Y., Galle, B., Panday, A., Hodson, E., Prinn, R., Wang, S., 2009. Observations of high rates of NO<sub>2</sub>-HONO conversion in the nocturnal atmospheric boundary layer in Kathmandu, Nepal. *Atmos. Chem. Phys.* 9, 6401–6415.
- Zhang, W., Tong, S., Jia, C., Wang, L., Liu, B., Tang, G., Ji, D., Hu, B., Liu, Z., Li, W., Wang, Z., Liu, Y., Wang, Y., Ge, M., 2020. Different HONO sources for three layers at the urban area of Beijing. *Environ. Sci. Technol.* 54, 12870–12880. <https://doi.org/10.1021/acs.est.0c02146>.
- Zhang, S., Sarwar, G., Xing, J., Chu, B., Xue, C., Sarav, A., Ding, D., Zheng, H., Mu, Y., Duan, F., Ma, T., He, H., 2021. Improving the representation of HONO chemistry in CMAQ and examining its impact on haze over China. *Atmos. Chem. Phys.* 21, 15809–15826. <https://doi.org/10.5194/acp-21-15809-2021>.
- Zhang, W., Tong, S., Jia, C., Ge, M., Ji, D., Zhang, C., Liu, P., Zhao, X., Mu, Y., Hu, B., Wang, L., Tang, G., Li, X., Li, W., Wang, Z., 2022. Effect of different combustion processes on atmospheric nitrous acid formation mechanisms: winter comparative observation in urban, suburban and rural areas of the North China Plain. *Environ. Sci. Technol.* 56, 4828–4837. <https://doi.org/10.1021/acs.est.1c07784>.
- Zhang, W., Tong, S., Lin, D., Li, F., Zhang, X., Wang, L., Ji, D., Tang, G., Liu, Z., Hu, B., Ge, M., 2023. Atmospheric chemistry of nitrous acid and its effects on hydroxyl radical and ozone at the urban area of Beijing in early spring 2021. *Environ. Pollut.* 316, 120710 <https://doi.org/10.1016/j.envpol.2022.120710>.
- Zheng, G., Su, H., Wang, S., Andreae, M.O., Pöschl, U., Cheng, Y., 2020. Multiphase buffer theory explains contrasts in atmospheric aerosol acidity. *Science*. 369, 1374–1377.